DERIVATION OF FOREST PARAMETERS FROM STEREOGRAPHIC UAV DATA – A COMPARISON WITH AIRBORNE LIDAR DATA

Christian Thiel, Christiane Schmullius

Department for Earth Observation, Friedrich-Schiller University Jena, Loebdergraben 32, 07743 Jena, Germany, E-Mail: Christian.Thiel@uni-jena.de, C.Schmullius@uni-jena.de

ABSTRACT

In this study unmanned aerial vehicle (UAV) image (photograph) based point clouds and products were compared to airborne LiDAR based data and products over a forested area. The test site is located in Germany, 15 km southeast of Jena. A total area of approximately 175 ha was covered during a UAV flight campaign. For this study, a subset of 4 ha (200 m x 200 m) was defined. The UAV-LiDAR comparison was accomplished at three different data levels: 1.) Point-like level (raster of maxima), 2.) Surface level (canopy height models - CHM), and 3.) Tree level (detection rate). In general, a high match between LiDAR and UAV based data/products was observed. The UAV data exhibits more details which is of particular importance for the detection of small trees. While using LiDAR data 45 out of 205 trees were not detected, only 14 trees were missed out when UAV data was used.

1. INTRODUCTION

The utilisation of UAVs for the acquisition of ultra-high resolution imagery has heavily increased during the past five years. Once the hardware is purchased, images can be recorded almost at any time and at low cost. The image parameters can be determined in terms of spectral channels, image overlap, and geometric resolution [1]. The overlap between the images enables stereoscopic image processing, the delineation of point clouds and the generation of seamless image mosaics. UAV image data products have gathered high interest in the forestry community [2-5].

Our major goal is to delineate several forest parameters such as canopy height, canopy cover, tree location, number of trees, tree density, tree height, stem volume, and tree species to create high quality reference data to investigate the impact of forest structure on Synthetic Aperture Radar (SAR) backscatter. Commonly, forest inventory does not contain the required details for this kind of investigation.

The main aim of this study is to evaluate the quality of UAV image based point clouds over forest. For this assessment the UAV data was compared to LiDAR data, as the spatial distribution of uncertainty cannot be assessed by the UAV data itself [6, 7]. A direct pointwise comparison with LiDAR is not feasible. Hence, we compared the data at three different levels: 1.) At point-like level employing one raster each featuring the elevation of the highest point within the cell. 2.) At surface level employing both CHMs. For this step, pit-free CHM models were delineated. Due to the differing data characteristics of UAV and LiDAR differing processing parameters had to be used, which might bias the direct comparison. Nevertheless, CHMs are important products as they form the base for many applications and higher level products. 3.) At tree level, were the commission and omission rates of a tree detection algorithm were compared for both data sets.

2. STUDY AREA

The study area is part of the Roda-River catchment, which is located 15 km southeast of the city of Jena, Germany (Figure 1 and Figure 2). The forest in the study area is intensively managed. The main tree species are spruce and pine, larch and birch occur as well. Most forest stands are homogeneous in terms of species composition and tree age, the tree density of the older stands shows a high degree of variability in part. Forest inventory data is available for many stands. However, it only provides stand-wise averages of relevant information (such as tree height, species compositions, relative stocking etc.).

Figure 1. Roda catchment (green polygon)

The study area features gentle terrain with elevations between 300 m and 400 m. The underlying bedrock (Early Trias – bunter), causes slightly acidic soils.

The presented results are based on a subset of the study area covering 4 ha (200 m x 200 m) of forest. For a part of this subset terrestrial laser scanner (TLS) data was acquired. This data was used to validate some of the results.

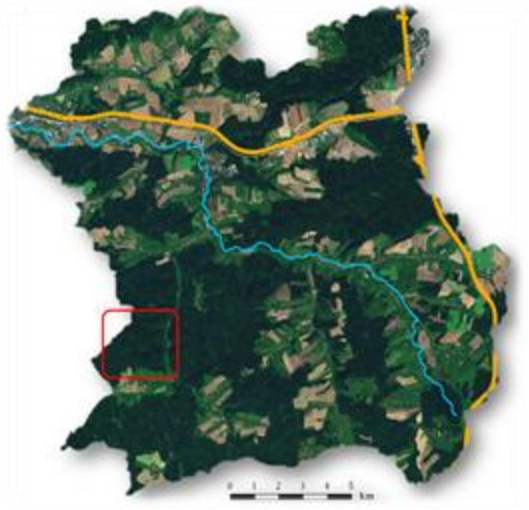

Figure 2. Catchment of the Roda-River. The red polygon frames the UAV flight campaign area

3. DATA

3.1. UAV data

Due to technical and legal restrictions, the study area (flight campaign area) was subdivided into seven sectors. Each of the sectors covers an area of approximately 25 ha. The flight duration was 7-10 minutes for each sector; the flight speed was set to 8 ms^{-1}. The flight route was planned and uploaded to the UAV before take-off. After take-off the UAV was switched to autopilot mode. To ensure intervisibility with the UAV X8000 (*Figure 3*), a platform at the height of the treetops carrying the pilot was necessary. The platform was provided by the voluntary fire brigade of Stadtroda, who made their turntable fire-escape ladder truck including staff available.

Figure 3. Logo-Team Geocopter X8000

For the orthorectification several teflon targets were distributed over the flight sectors (see Figure 4, ca. 5 m in front of the fire truck). The location of the targets was determined using DGPS. Table 1 summarizes the acquisition parameters of the UAV data. We acquired RGB (Figure 4) and multispectral (Figure 5) images. This study is based on the RGB data only.

TABLE 1: Details of UAV data acquisitions

Acquisition date	09th September 2014
Weather	14°C, calm, mostly cloudless
Instruments	Sony NEX-7 (*f* 19 mm, 1/400 s, ISO200) Tetracam mini MCA 2 ILS, Filters: Blue, Green, Red, Red Edge, Near Infrared
Platform	Logo-Team Geocopter X8000
Flight altitude	100 m over treetops
Area covered	175 ha (7 flights per camera)
Overlap	80% in flight direction 60% between parallel tracks
Number of images	Sony NEX-7: 1,750 Tetracam mini MCA: 2 5,200
Resolution	NEX-7: 2 cm (on ground) miniMCA: 8 cm (on ground)

Figure 4. Sony NEX-7 RGB data example

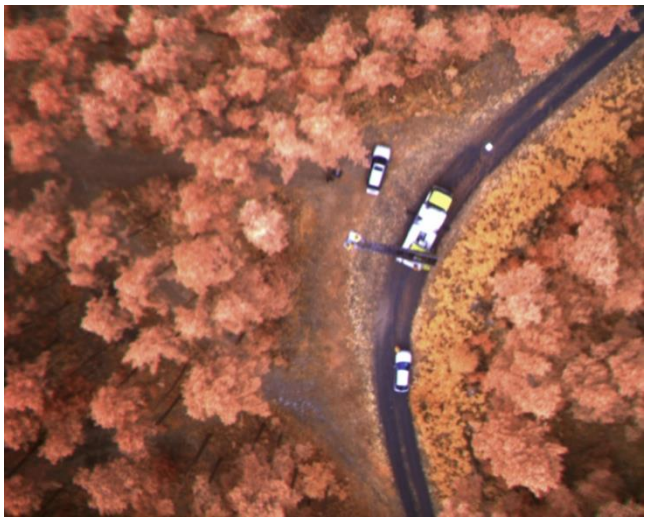

Figure 5. Tetracam miniMCA2 data (NIR/RedEdge/Green)

Image mosaics and point clouds were delineated using structure from motion (SfM) techniques as implemented in Agisoft Photoscan 1.2.4 [8]. The internal processing steps

involve a) the detection of stable points (for differing viewpoints and lighting) in the images, b) the generation of descriptors for each point to find correspondences across the images, c) resolving camera orientation parameters, d) finding camera locations using a bundle-adjustment, and e) dense surface reconstruction and texture mapping. According to Agisoft (personal communication) several implemented processes are based on previous publications. Though, PhotoScan is commercial software and the code is not published.

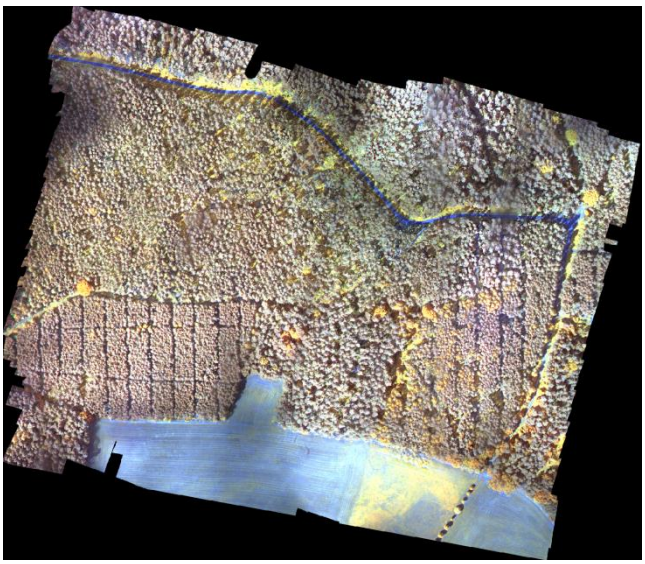

Figure 6. Tetracam mini MCA2 image mosaic of flight sector 1 (NIR/RedEdge/Green, ca. 450 m x 550 m)

The user driven PhotoScan processing includes image alignment and generation of a sparse point cloud, georeferencing the data using DGPS measurements, refinement of image alignment, filtering of sparse point cloud and elimination of erroneous points, and generation of a dense point cloud and image mosaics. Figure 6 shows an image mosaic based on 490 Tetracam mini MCA2 images. A natural color point cloud example is given in Figure 7. The RGB point clouds feature approximately 80,000,000 points per flight sector which corresponds to 310 points/m². Figure 8 depicts the UAV point cloud of the 4 ha subset of flight sector 1.

Figure 7. Detail view of Sony NEX-7 RGB image data based point cloud (natural color)

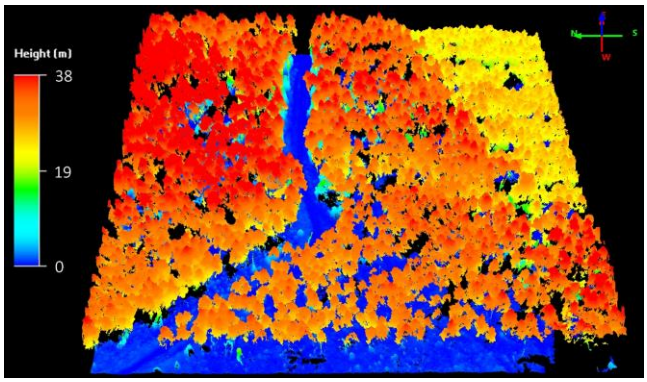

Figure 8. Subset (4 ha, 200 m x 200 m) of Sony NEX-7 image data based point cloud. Mind that North is to the left.

3.2. LiDAR data

The LiDAR data was acquired in the same year as the UAV data, however at a different season (winter). Although non-deciduous trees are dominant in the 4 ha subset, the matter might impact some of the results of this study. Figure 9 shows the same subset as Figure 8. The lower point density of the LiDAR data (4-8 points/m²) is clearly visible. Bright areas (left and right side) occur were two LiDAR tracks overlap (8 points/m²). Table 2 summarizes the key parameters of the LiDAR data.

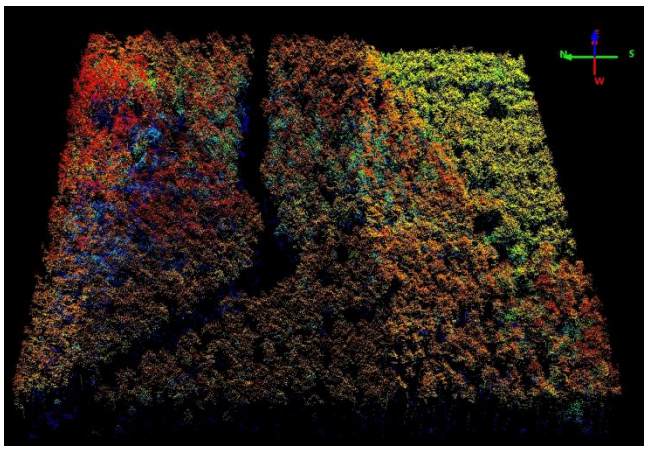

Figure 9. Subset of LiDAR data (non-ground points)

TABLE 2: Details of LiDAR data acquisitions

Acquisition date	15th February 2014
Instrument	Optech ALTM Gemini
Point density	4-8 points/m²
Footprint diameter	0.15 – 0.25 m
Height RMS	< 0.08 m
Platform	Cessna 208 Caravan
Flight altitude	approximately 1000 m above ground
Points classes	ground & non-ground, each subdivided into first, last, only
Supplier	Thuringian land surveying office

3.3. TLS data

TLS data is used for forestry applications for about 15 years. Using this technique the forest can be scanned rapidly in millimetre-level detail [9]. Our TLS campaign was conducted at the same day as the UAV flights. Nine scan positions set up within the area of the 4 ha subset. At each of the positions two scans were conducted (one horizontal and one vertical). This approach led to a very dense coverage of stems, undergrowth, and canopy. For the coregistration of the individual scans artificial reflectors were installed. The scanner positions were determined by Differential Global Navigation Satellite System (dGNSS) and conventional surveying (trigonometric surveying). The key parameters of the TLS data are summarized in Table 3.

TABLE 3: Details of LiDAR data acquisitions

Acquisition date	09th September 2014
Instrument	Riegl VZ 1000
Area	220 m x 165 m
Number of scan positions	9 (one horizontal and one vertical scan per position)
Angular resolution	0.02 and 0.04 degrees
Number of points	432,026,502
Positional uncertainty of single scans (relative)	0.005 m to 0.016 m (1 sigma)
Positional uncertainty of single scans (absolute)	2.5 cm (1 sigma), precision better than 1.0 cm

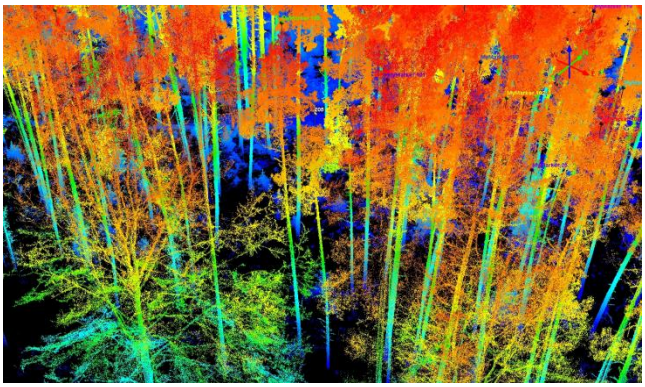

Figure 10. Data example of Riegl VZ 1000 TLS data acquired within subset

By means of the TLS point cloud the position of 205 trees was manually detected and labelled. These trees were used as reference for the validation of the tree detection rate.

4. METHODS

The processing of the point clouds was conducted using the software package LASTools (version from 02/2016). First of all, the LiDAR and UAV point clouds were normalized for terrain. The terrain height was determined from the LiDAR ground returns using the pulses being classified as last or only. Secondly, all points below zero and above 50 m were eliminated.

4.1. Generation of raster data from point clouds

The direct comparison of UAV and LiDAR points is not feasible, as the center position of two corresponding points (one LiDAR and one UAV point) and the footprint of the points are differing. Consequently, for comparing LiDAR and UAV data, quadratic raster were generated. The values of the raster cells were set to the height of the highest point within each cell. With regard to the LiDAR data only non-ground points (first and only) were used. If no point lies within a cell the raster value was left empty (no data).

The cell size was 0.25 m x 0.25 m for the LiDAR data and 0.10 m x 0.10 m for the UAV data. Thus, the LiDAR cell size roughly corresponds to the coverage of one LiDAR footprint. Due to the maximum point density of 8 points/m² it is unlikely that more than one LiDAR points lies within one raster cell. According to the average UAV point density of 310 points/m² the average number of points per UAV raster cell is 3.1. The approach of selecting the maximum value within one cell might result in a slight bias towards greater heights in the UAV raster, when compared to the LiDAR raster. Nevertheless, this strategy was chosen to derive raster representing the top of the canopy.

The rasterization causes a reduction of the geolocation accuracy of the points. The theoretical maximum deviation of point coordinate and raster coordinate equals one half of the diagonal of one raster cell, i.e. 0.178 m for the LiDAR case. The reduction of geolocation accuracy can result in a slight reduction of the correlation magnitude between UAV and LiDAR, but it does not introduce a bias.

4.2. Generation of CHMs from point clouds

Canopy height models (CHM) are used as input for many forestry related data products. For example, several tree detection algorithms are based on CHMs [10-12]. Some of these algorithms provide better results, when CHMs without pits within one tree crown (pit-free) are used. For this reason, we decided to use the approach suggested by [13], which is implemented in the LASTools software. The final geometric resolution of the LiDAR data was 0.25 m and 0.05 m for the UAV data. The relationship between LiDAR and UAV resolution roughly represents the relationship of the point densities. The chosen resolutions might cause slight oversampling, which was preferred against loosing information. The maximum interpolation distance for both datasets was set to 1 m. The LASTools parameter *spike_free*, which steers the magnitude of the pit-filter, was set to 1.5 for the LiDAR and 0.5 for the UAV data.

4.3. Tree detection

Tree detection was accomplished based on the previously delineated pit-free CHMs. The chosen algorithm searches for the local maximum within the search window, while the dimensions of the search window are steered by the CHM height [14]. This algorithm is implemented in the *CanopyMaxima* function of the FUSION software [15]. Alt-

hough relatively simple, this approach showed good results when compared to other methods [11, 12]. The relationship between the search window size and the CHM was adjusted to the forest characteristics of the 4 ha subset by estimating the tree height (h_t) – crown diameter (d_t) relationship using the TLS data. Both parameters were measured manually for the 205 detected trees. Based on these measurements the following empirical equation (1) was established:

$$d_t = 0.003028 h_t^2 + 0.063312 h_t \quad (1)$$

The coefficient of determination (R^2) for (1) was 0.81. The other parameters of *CanopyMaxima* were set as follows; LiDAR: *res* = 2.0, *mult* = 1.0, UAV: *res* = 0.625, *mult* = 1.0. The minimum tree height was 10 m.

5. EXPERIMENTAL OBSERVATIONS

5.1. Rasterized point clouds

Figure 11 and Figure 12 show overlays of the UAV and the LiDAR raster, were in both cases the LiDAR raster is the upper layer. No data pixels are transparent. As the LiDAR raster features a high number of no data pixels (> 50%), a large partition of the UAV data is visible. The effect of the high partition of no data pixels in the LiDAR data is evident in the outer frame of Figure 11. This figure shows a part of the test site, which is slightly greater than the 4 ha subset. For the outer frame, only LiDAR raster data is available, while for the 4 ha subset LiDAR and UAV data are shown.

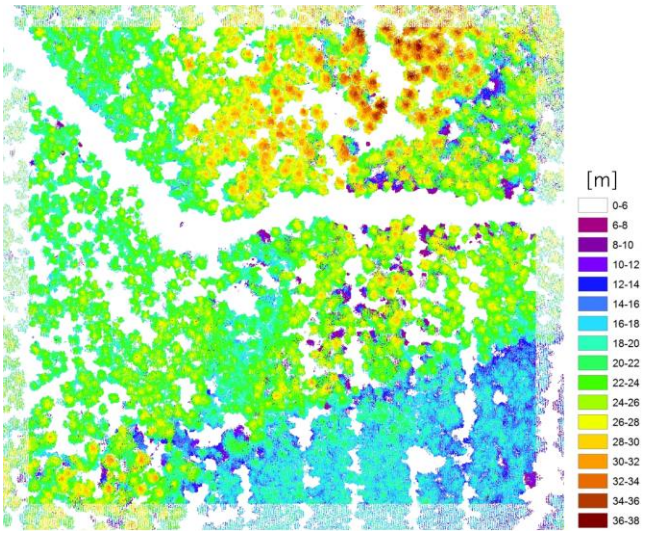

Figure 11. Rasterized UAV and LiDAR point clouds using highest point within raster cell. Upper layer: LiDAR raster. Lower layer: UAV raster. Mind the "frame" were only LiDAR data is available.

As the same legend for LiDAR and UAV was applied, the LiDAR pixels are not distinguishable when they feature the same height as the UAV pixels. This effect becomes obvious when viewing Figure 12 which depicts the raster for a single tree crown. In overall, LiDAR data and UAV data show good agreement. However, some LiDAR pixels feature a much smaller height compared to the UAV raster. Obviously, some LiDAR shots are capable to penetrate through the canopy and are reflected at lower branches. On the other hand, there might be gaps in the canopy which are not detectable by the UAV data. Thus, there might be dissimilarities caused by the different acquisition systems (passive vs. active, stereogrammetry-like vs. direct measurement etc.). Furthermore, the different acquisition season might have some impact, even though Figure 12 shows a non-deciduous tree.

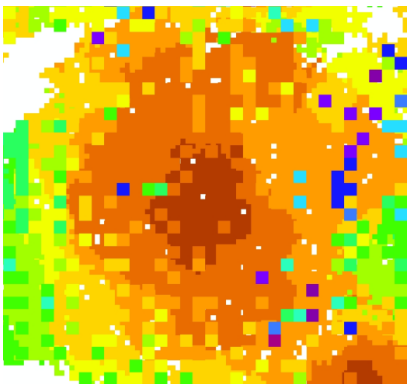

Figure 12. Data example of rasterized point clouds for one tree. The (coarser) LiDAR pixels are visible when they feature a different height than the underlying UAV pixels.

The good agreement between both dataset is demonstrated by Figure 13. This scatterplot considers all pixels with heights greater 10 m. Some of the clutter is due to the different geometric resolutions of both raster. Also, the previously discussed issues cause clutter. Nevertheless, the correlation is high (r = 0.89).

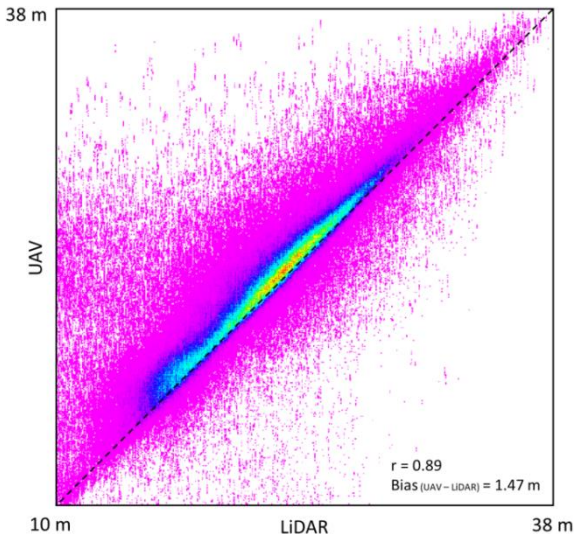

Figure 13. Scatterplot LiDAR vs. UAV based on raster for the 4 ha subset

In overall, the UAV based heights are 1.5 m higher than the LiDAR heights. One reason for this observation might be related to the different acquisition systems and different seasons as discussed above. Another reason goes back to the delineation of the raster as discussed in section 4.1. The LiDAR reflection is registered at the sensor when the reflected energy exceeds a defined threshold. Small objects, such as twigs that constitute only a minor fraction within the LiDAR footprint might not cause sufficient reflection for a distance measurement, while such objects can be resolved by the UAV data. Eventually, part of the bias can be explained by tree growth during the seven months between the acquisitions.

5.2. Canopy height model

Figure 14 shows the UAV data based CHM for the 4 ha subset. This subset contains clusters with large trees (top of the image) and also an area with small trees (bottom). The higher point density of the UAV data might be of particular interest for areas with small trees and small-sized crowns.

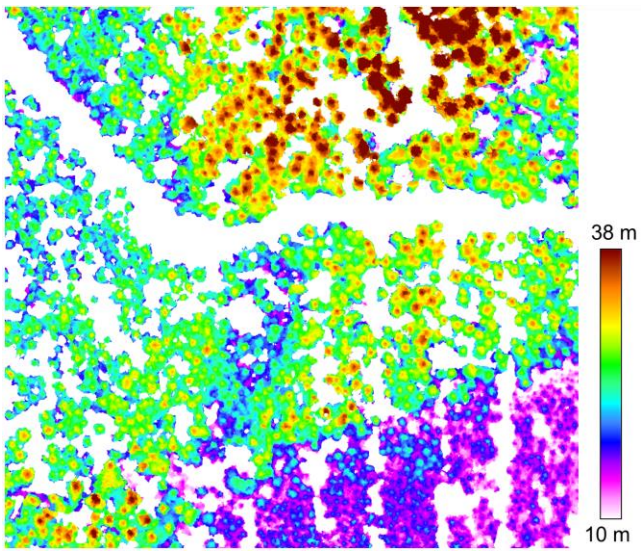

Figure 14. UAV data based CHM of the 4 ha subset

Figure 15 and Figure 16 show an enlarged subset featuring small trees. The comparison of both figures reveals the higher degree of details in the UAV data based CHM (Figure 16). Some structures and patterns in Figure 15 (LiDAR) cannot be clearly related with single tree crowns, while the UAV data provides sufficient details for the visual recognition of those trees.

Accordingly, the difference image LiDAR–UAV (not provided) primarily reveals differences in areas with small trees. Additionally, in the UAV data the treetops are slightly higher compared to the LiDAR CHM. Due to the very high point density of the UAV data most of the treetops are captured in detail, while treetops are missed out regularly by the LiDAR shots.

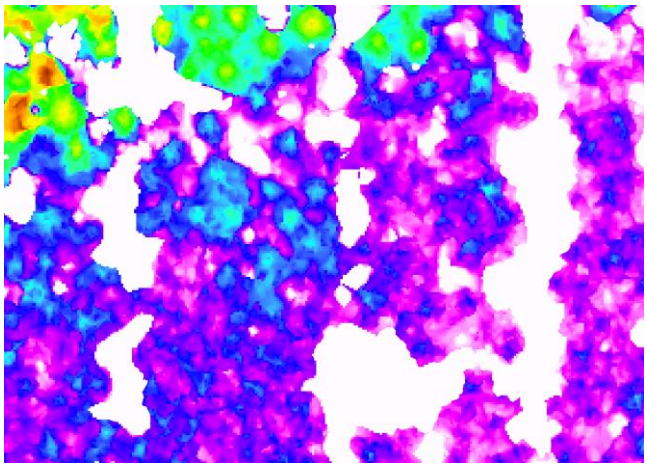

Figure 15. Section (60 m x 40 m) of LiDAR based CHM featuring small trees. The small trees can be hardly discriminated.

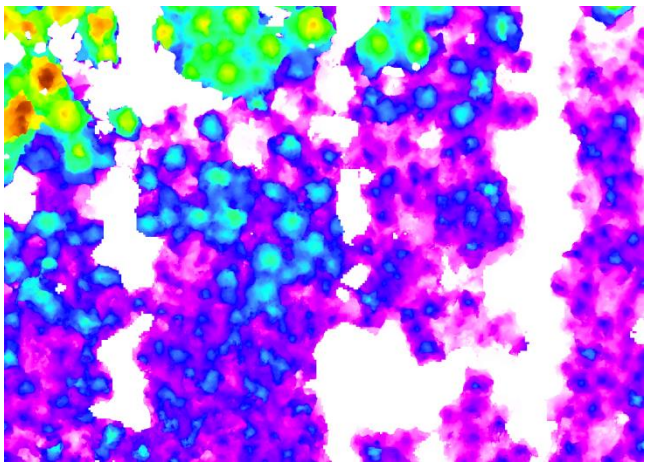

Figure 16. Section (60 m x 40 m) of UAV based CHM. UAV data shows more details compared to LiDAR.

Nevertheless, both CHMs show a great agreement, as indicated by the scatterplot (Figure 17). Part of the clutter is due to the different resolutions of both datasets and the higher degree of details in the UAV data. The bias is smaller compared to point-like comparison (Figure 13), as for the UAV CHM all points were considered instead of using the maximum point within one raster cell only. Still, the UAV heights are 0.85 m increased against the LiDAR heights. Due to the smaller point density the LiDAR might miss out the highest features of a tree (e.g. treetop), while this feature is preserved in the UAV data. Also, small objects might not cause sufficient reflection which results in some penetration of the LiDAR pulse into the canopy, while the UAV based point clouds represent the top of the canopy. Again, seasonal effects and in particular tree growth certainly have some impact.

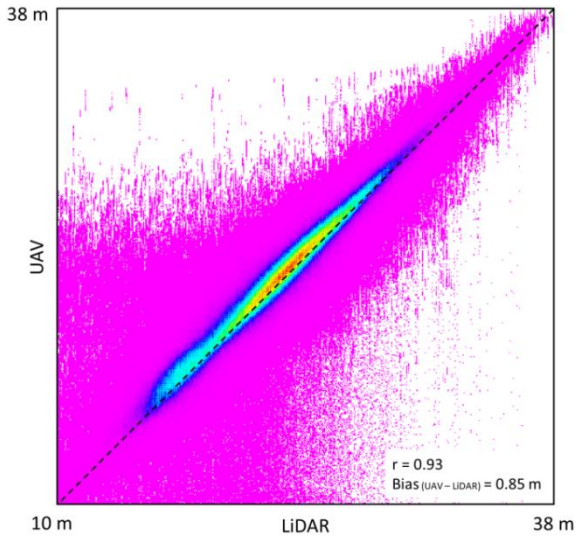

Figure 17. Scatterplot LiDAR vs. UAV based on CHMs for the 4 ha subset

5.3. Tree detection

For the 4 ha subset in total 1,789 trees were detected based on the LiDAR CHM, while 2,115 trees could be delineated using the UAV CHM. Figure 18 shows the position of the detected trees. In many cases, LiDAR and UAV detect the same potential tree.

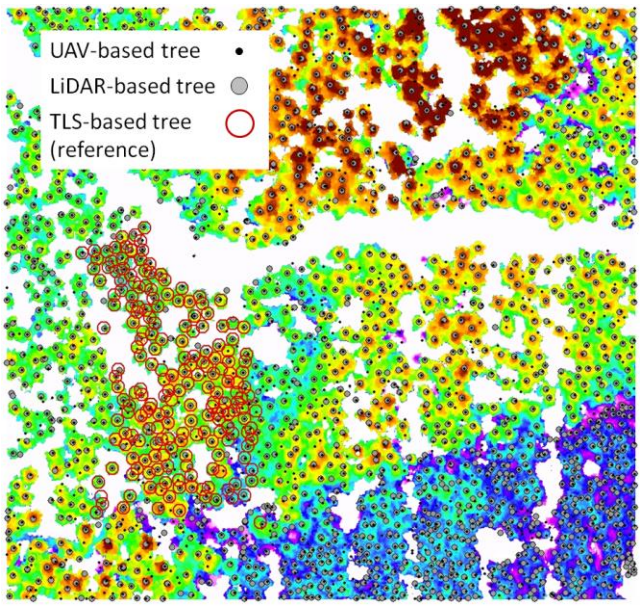

Figure 18. Delineated tree positions over UAV CHM

The detection rates and the commission errors were computed using the manually determined TLS-based positions of 205 trees. Compared to the remaining subset the reference trees exhibit an average height and crown diameter. A tree was counted as detected when the tree position was located within the 1.5 m radius of the reference tree position. The results are as follows:

LiDAR
Detection rate: 78.0% (45 trees missing)
Commission: 9.8% (20 trees)

UAV
Detection rate: 93.2% (14 trees missing)
Commission: 10.7% (22 trees).

The commission (false positive detection) is similar for both datasets. Thus, the comparison of the detection rate is justified. The detection rate using UAV data is 15% higher compared to LiDAR which is due to the higher level of details in the UAV CHM. False positive detections occurred primarily when major branches were extending into a canopy gap. Another source of false detections is small trees with two treetops. In several cases the same false detection (the same false tree) occurred in the LiDAR and UAV case. Most of the missed out trees are small trees located very close to a large tree. In this case, the crowns of both trees are almost connected. More sophisticated tree detection algorithms, in particular point based approaches, might be capable to delineate some of these partly hidden trees [10, 11, 16-18]. For the scope of this data driven study the selected tree detection algorithm was sufficient.

6. SUMMARY, CONCLUSIONS AND OUTLOOK

In general, good agreement between LiDAR and UAV based data and products has been observed. Compared to LiDAR, UAV data provides more geometrical details and thus leads to improved tree detection. The UAV based data features slightly greater heights compared to the LiDAR data. As discussed in the results, this observation can be explained by four major reasons: 1.) The much higher point density in the UAV data (LiDAR pulses might miss out the highest tree elements), 2.) The slight penetration of the LiDAR pulse into the canopy (small objects such as a small branches might not cause sufficient reflection), 3.) The increased penetration of the LiDAR pulse due to data acquisition in winter, and 4.) Tree growth in the seven months period between LiDAR and UAV data acquisition.
According to the above findings UAV image data can be an alternative for areas where no LiDAR data is available or frequent acquisitions are required.
This study will be extended to a larger area including broad leafed trees and a higher number of reference trees. Furthermore, the height accuracy of the delineated trees will be investigated. This step as well as the tree detection accuracy will be conducted separately for various height classes.

7. ACKNOWLEDGEMENT

The technical equipment (UAV, DGPS devices, and TLS) was facilitated by the former TMBWK (Thuringian Ministry for Education, Science, and Culture) and the European Fond for Regional Development (EFRE) (FK 13007-715). The authors would like to thank Dr. J. Baade for the TLS measurements and the TLS data preprocessing. Last but not least: this work would not have been possible without the

voluntary fire brigade of Stadtroda. Thank you very much for providing and operating your turntable fire-escape ladder truck!

8. REFERENCES

1. Suomalainen, J., Anders, N., Iqbal, S., Roerink, G., Franke, J., Wenting, P., Hünniger, D., Bartholomeus, H., Becker, R., & Kooistra, L. (2014). *A Lightweight Hyperspectral Mapping System and Photogrammetric Processing Chain for Unmanned Aerial Vehicles*, Remote Sensing, vol. 6, pp. 11013-11030.

2. Hernández-Clemente, R., Navarro-Cerrillo, R., Ramírez, F., Hornero, A., & Zarco-Tejada, P. (2014). *A Novel Methodology to Estimate Single-Tree Biophysical Parameters from 3D Digital Imagery Compared to Aerial Laser Scanner Data*, Remote Sensing, vol. 6, pp. 11627-11648.

3. Puliti, S., Olerka, H., Gobakken, T., & Næsset, E. (2015). *Inventory of Small Forest Areas Using an Unmanned Aerial System*, Remote Sensing, vol. 7, pp. 9632-9654.

4. Zarco-Tejada, P. J., Diaz-Varela, R., Angileri, V., & Loudjani, P. (2014). *Tree height quantification using very high resolution imagery acquired from an unmanned aerial vehicle (UAV) and automatic 3D photo-reconstruction methods*, European Journal of Agronomy, vol. 55, pp. 89-99.

5. Chianucci, F., Disperati, L., Guzzi, D., Bianchini, D., Nardino, V., Lastri, C., Rindinella, A., & Corona, P. (2016). *Estimation of canopy attributes in beech forests using true colour digital images from a small fixed-wing UAV*, International Journal of Applied Earth Observation and Geoinformation, vol. 47, pp. 60-68.

6. Jalobeanu, A. & Gonçalves, G. (2015). *The Unknown Spatial Quality of Dense Point Clouds Derived From Stereo Images*, IEEE Transactions on Geoscience and Remote Sensing Letters, vol. 12, pp. 1013-1017.

7. Mader, D., Blaskow, R., Westfeld, P., & Maas, H. G. (2015). *UAV-BASED ACQUISITION OF 3D POINT CLOUD –A COMPARISON OF A LOW-COST LASER SCANNER AND SFM-TOOLS*, ISPRS - International Archives of the Photogrammetry, Remote Sensing and Spatial Information Sciences, vol. XL-3/W3, pp. 335-341.

8. LLC, A., "Agisoft PhotoScan User Manual - Professional Edition, Version 1.2," ed. St. Petersburg, Russia, 2016.

9. Liang, X., Kankare, V., Hyyppä, J., Wang, Y., Kukko, A., Haggrén, H., Yu, X., Kaartinen, H., Jaakkola, A., Guan, F., Holopainen, M., & Vastaranta, M. (2016). *Terrestrial laser scanning in forest inventories*, ISPRS Journal of Photogrammetry and Remote Sensing, vol. 115, pp. 63-77.

10. Zhen, Z., Quackenbush, L., & Zhang, L. (2016). *Trends in Automatic Individual Tree Crown Detection and Delineation—Evolution of LiDAR Data*, Remote Sensing, vol. 8, p. 333.

11. Kaartinen, H., Hyyppä, J., Yu, X., Vastaranta, M., Hyyppä, H., Kukko, A., Holopainen, M., Heipke, C., Hirschmugl, M., Morsdorf, F., Næsset, E., Pitkänen, J., Popescu, S., Solberg, S., Wolf, B. M., & Wu, J.-C. (2012). *An International Comparison of Individual Tree Detection and Extraction Using Airborne Laser Scanning*, Remote Sensing, vol. 4, pp. 950-974.

12. Edson, C. & Wing, M. G. (2011). *Airborne Light Detection and Ranging (LiDAR) for Individual Tree Stem Location, Height, and Biomass Measurements*, Remote Sensing, vol. 3, pp. 2494-2528.

13. Khosravipour, A., Skidmore, A.K., Isenburg, M. and Wang, T.J. (2015). Development of an algorithm to generate pit-free Digital Surface Models from LiDAR,, presented at the SilviLaser La Grande Motte, France.

14. Popescu, S. C. & Wynne, R. H. (2004). *Seeing the trees in the Forest: Using Lidar and Multispectral Data Fusion with Local Filtering and Variable Window Size for Estimating Tree Height*, Photogrammteric Engineering & Remote Sensing, vol. 70, pp. 589-604.

15. McGaughey, R. J., "FUSION/LDV: Software for LIDAR Data Analysis and Visualization," USDA - Pacific Northwest Research Station, United States2015.

16. Liu, T., Im, J., & Quackenbush, L. J. (2015). *A novel transferable individual tree crown delineation model based on Fishing Net Dragging and boundary classification*, ISPRS Journal of Photogrammetry and Remote Sensing, vol. 110, pp. 34-47.

17. Mongus, D. & Žalik, B. (2015). *An efficient approach to 3D single tree-crown delineation in LiDAR data*, ISPRS Journal of Photogrammetry and Remote Sensing, vol. 108, pp. 219-233.

18. Jakubowski, M., Li, W., Guo, Q., & Kelly, M. (2013). *Delineating Individual Trees from Lidar Data: A Comparison of Vector- and Raster-based Segmentation Approaches*, Remote Sensing, vol. 5, pp. 4163-4186.